Cerebral Cortex, December 2021;31: 5308–5318

https://doi.org/10.1093/cercor/bhab159
Advance Access Publication Date: 28 June 2021
Original Article

ORIGINAL ARTICLE

The Organization of Frontostriatal Brain Wiring in Healthy Subjects Using a Novel Diffusion Imaging Fiber Cluster Analysis

J. J. Levitt[1,2,3], F. Zhang[4], M. Vangel[5], P. G. Nestor[1,2,6], Y. Rathi[3,5], M. Kubicki[3,4,5], M. E. Shenton[3,4,5] and L. J. O'Donnell[4]

[1]Department of Psychiatry, VA Boston Healthcare System, Brockton Division, Brockton MA 02301, USA, [2]Department of Psychiatry, Harvard Medical School, Boston, MA 02115, USA, [3]Department of Psychiatry, Psychiatry Neuroimaging Laboratory, Brigham and Women's Hospital, Harvard Medical School, Boston, MA 02215, USA, [4]Department of Radiology, Brigham and Women's Hospital, Harvard Medical School, Boston, MA 02115, USA, [5]Department of Psychiatry, Massachusetts General Hospital, Harvard Medical School, Boston, MA 02114, USA and [6]Department of Psychology, University of Massachusetts, Boston, MA 02125, USA

Address correspondence to James J. Levitt, M.D., Department of Psychiatry-116A, VA Boston Healthcare System, Harvard Medical School, 940 Belmont Street, Brockton, MA 02301, USA. Email: james_levitt@hms.harvard.edu

Abstract

To assess normal organization of frontostriatal brain wiring, we analyzed diffusion magnetic resonance imaging (dMRI) scans in 100 young adult healthy subjects (HSs). We identified fiber clusters intersecting the frontal cortex and caudate, a core component of associative striatum, and quantified their degree of deviation from a strictly topographic pattern. Using whole brain dMRI tractography and an automated tract parcellation clustering method, we extracted 17 white matter fiber clusters per hemisphere connecting the frontal cortex and caudate. In a novel approach to quantify the geometric relationship among clusters, we measured intercluster endpoint distances between corresponding cluster pairs in the frontal cortex and caudate. We show first, the overall frontal cortex wiring pattern of the caudate deviates from a strictly topographic organization due to significantly greater convergence in regionally specific clusters; second, these significantly convergent clusters originate in subregions of ventrolateral, dorsolateral, and orbitofrontal prefrontal cortex (PFC); and, third, a similar organization in both hemispheres. Using a novel tractography method, we find PFC-caudate brain wiring in HSs deviates from a strictly topographic organization due to a regionally specific pattern of cluster convergence. We conjecture cortical subregions projecting to the caudate with greater convergence subserve functions that benefit from greater circuit integration.

Key words: brain wiring, caudate, diffusion magnetic resonance imaging, prefrontal cortex, tractography

Introduction

The cortical–subcortical basal ganglia network, which contains the frontostriatal circuits, importantly influences higher cognitive brain functions because its subcortical thalamic output targets cognitive and limbic regions in the prefrontal cortex as well as motor regions in the frontal cortex. This allows the basal ganglia to modulate nonmotor cognitive and emotional functions in addition to motor function (Alexander et al. 1986; Alexander and Crutcher 1990; Manoach et al. 2000). It is believed that functional areas of the cortex project in a generally topographic manner to the striatum (Alexander et al. 1990) Consequently, the striatum has been divided into three functional zones: limbic, associative, and sensorimotor based on its pattern of connectivity with cortical functional areas. These basal ganglia topographic projections have been conceptualized as forming three spatially and functionally segregated corticostriatal–thalamic feedback subloops (Voorn et al. 2004). Abnormalities affecting the white matter corticostriatal circuit projections or the gray matter basal ganglia circuit structures affecting any of the three subloops could lead to dysfunction of the entire subloop and adversely affect cognitive, affective, or sensorimotor function (Cummings 1993; Bhatia and Marsden 1994; Calabresi et al. 1997; Levitt et al. 2002; Levitt et al. 2010; Levitt et al. 2017).

Cortical axonal fiber projections to the striatum, however, are not exclusively topographically arranged (e.g., Haber 2003; Haber 2010; Averbeck et al. 2014). Such projections have been shown to project in both a functionally segregated, anatomically topographic pattern, but also in a functionally integrative, anatomically, nontopographic pattern yielding segregated projection and overlapping projection zones, respectively. Animal tract tracing and human imaging studies (Haber 2003; Lehericy et al. 2004; Draganski et al. 2008; Averbeck et al. 2014) both support the existence of corticostriatal projection patterns yielding integrative and segregated corticostriatal target zones. The function of striatal target zones that receive overlapping cortical projections is to allow for the integration of information from different cortical functional subregions (e.g., Haber 2003; Haber 2010).

Diffusion magnetic resonance imaging (dMRI) tractography is a promising technique that provides a method to measure the local variation in brain connectivity patterns in human subjects, in vivo (Basser and Pierpaoli 1996; Mori et al. 1999; Westin et al. 1999; Basser et al. 2000). We have developed two novel ways of using dMRI tractography to measure the local variation in frontostriatal connectivity patterns in human subjects. First, in prior work based on frontostriatal tractography–derived streamline counts, we labeled striatal surface voxels into mixed, or dominant-input categories based on their connectivity patterns with the frontal cortex (Levitt et al. 2020). Voxels receiving at least 70% of their projections from one of four frontal regions of interest (ROIs) were labeled mixed, whereas those receiving fewer than 70% of streamline counts arising from any single frontal cortical region were labeled dominant-input. A finding of more mixed striatal surface voxels suggested a more integrative pattern of frontostriatal connectivity. Using this approach, we found that the pattern was less integrative in schizophrenia versus healthy controls (Levitt et al. 2020). Our focus on the projection zone pattern on the striatal surface rather than on diffusion measures of the axonal projections, themselves, was a novel use of dMRI tractography.

In the current study, we assessed healthy subjects in order to establish a normal wiring pattern, which we can later use to compare with other neuropsychiatric conditions. Here, we employed a second novel way of using tractography using a fiber clustering method. This approach utilizes machine learning to generate clusters of streamlines, or fibers, based on the similarity of their trajectories. With this approach, we identified and analyzed all fiber clusters connecting ROIs in the frontal cortex and the caudate from FreeSurfer (Fischl 2012) for their degree of geometric convergence. More specifically, to assess the geometry of the input from multiple fiber clusters, we measured the mean distance between the endpoints of streamlines of fiber clusters coming from frontal cortical ROIs (i.e., cortical distance) and the mean distance between the endpoints of the corresponding streamlines of fiber clusters projecting to the caudate (i.e., caudate distance; see Fig. 1*a*). We performed 2 analyses. First, we plotted the relationship between the cortical and the corresponding caudate endpoint distances for all 17 fiber cluster pairs to assess whether there was an overall linear relationship that would be expected in a strictly topographic pattern of projections, or if there were cluster-pairs that deviated from this pattern. Second, as we found that certain pairs of clusters were significantly convergent, and hence not parallel or strictly topographically organized, we then examined the pattern of convergence for each cluster with all other clusters within each hemisphere to detect from where in the frontal cortex such significantly convergent clusters emanated.

Although the two approaches differ, they are complementary approaches for assessing patterns of brain wiring. The first striatal surface voxel labeling method is suited for analyzing striatal surface voxel connectivity patterns (mixed, or dominant-input); the second fiber clustering method is suited for analyzing frontostriatal fiber, geometric, wiring patterns (e.g., whether anatomically convergent, or parallel). A finding of more mixed striatal surface voxels suggests a more integrative pattern of frontostriatal connectivity. Similarly, a finding of an anatomically more convergent fiber wiring pattern also suggests a pattern of greater circuit integration. We believe the two measures when applied to the same subjects, which we plan to do, will yield convergent findings. The striatal surface labeling method will identify where on the surface of the striatum there are mixed voxels and, thus, where there are striatal surface hubs. The fiber cluster method, on the other hand, will identify those ROIs in the frontal cortex that send out convergent fiber projections to the caudate, which allows for more "cross-talk" between frontal subregions.

Based on animal work (e.g., Averbeck et al. 2014) and our prior human work (Levitt et al. 2020), we hypothesized 1) that frontostriatal connectivity would deviate from a strictly anatomically topographic arrangement based on a pattern of greater convergence and 2) that such deviations characterized by greater convergence would be more localized to certain clusters coming from specific subregions of the frontal cortex, which we surmise may subserve functions that benefit from greater circuit integration. (e.g., Haber 2011; Rushworth et al. 2011).

Methods

Subjects

Hundred randomly selected young adult healthy subjects (HSs) from the Human Connectome Project (HCP) were used in this study. Data were downloaded from the HCP publicly available website (https://www.humanconnectome.org).

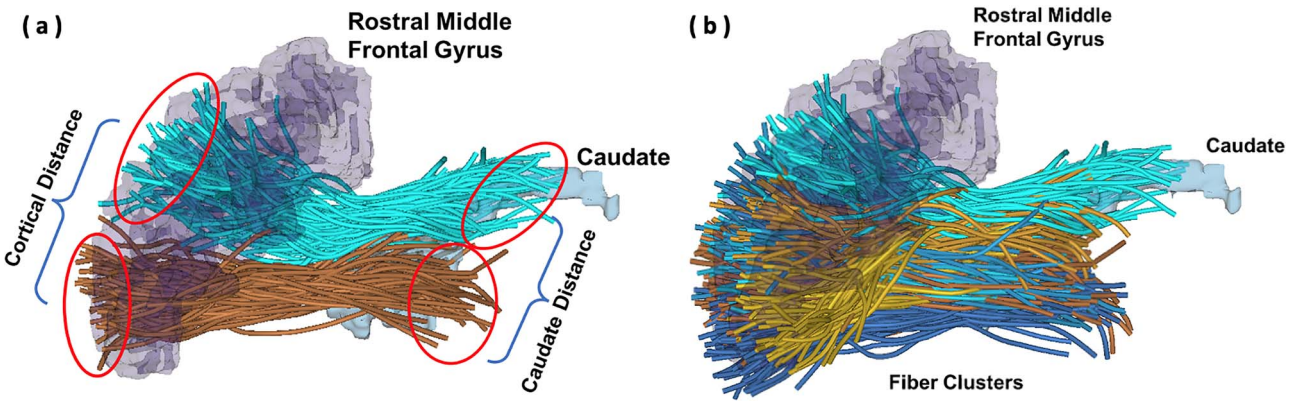

Figure 1. (*a*) 3D reconstruction of streamlines and regions of interest showing cortical and caudate intercluster endpoint distances between two frontostriatal fiber clusters projecting to the caudate from rostral middle frontal gyrus. (*b*) 3D reconstruction of streamlines showing multiple color-coded frontostriatal fiber clusters superimposed on one another.

Image Acquisition and Preprocessing

The HCP provides dMRI data that were acquired with a high-quality image acquisition protocol using a customized Connectome Siemens Skyra scanner and processed using a well-designed processing pipeline (Glasser et al. 2013) including motion correction, eddy current correction, and EPI distortion correction. The acquisition parameters of the dMRI data in HCP were TE = 89.5 ms, TR = 5520 ms, and voxel size = 1.25 × 1.25 × 1.25 mm^3. A total of 288 images were acquired in each dMRI dataset, including 18 baseline images with a low diffusion weighting $b = 5$ s/mm^2 and 270 diffusion-weighted (DW) images evenly distributed at three shells of $b = 1000/2000/3000$ s/mm^2. More detailed information about the HCP data acquisition and preprocessing can be found in Glasser et al. (2013).

Structural Image Postprocessing

Diffusion imaging two-tensor whole brain tractography postprocessing. We used the Unscented Kalman Filter (UKF)-based two-tensor tractography algorithm (Malcolm et al. 2010) to trace fiber paths throughout the whole brain (Malcolm et al. 2010; Rathi et al. 2010). The multitensor tractography algorithm (Malcolm et al. 2010) used in this work was judged as one of the best tractography algorithms in a "Fiber Cup" challenge held during MICCAI 2009 (Fillard et al. 2011). It allows to faithfully trace fibers through crossing regions while estimating the tensor parameters in a consistent manner. We extracted the $b = 3000$ shell of 90 gradient directions and all $b = 0$ scans for each subject, as applied in our previous studies that perform tractography-based analysis using HCP data (O'Donnell et al. 2017; Zhang et al. 2017; Zhang, Wu, Norton, et al. 2018c; Zhang, Wu, et al. 2019). Angular resolution is better and more accurate at high *b*-values such as 3000 (Descoteaux et al. 2007; Ning et al. 2015) and this single shell was chosen for reasonable computation time and memory use when performing tractography. Specifically, tractography was seeded in all voxels within the brain mask where fractional anisotropy (FA) was greater than 0.1. Tracking stopped where the FA value fell below 0.08 or the normalized mean signal (the sum of the normalized signal across all gradient directions, which was employed to robustly distinguish between white/gray matter and cerebrospinal fluid [CSF]) fell below 0.06, as suggested in (Zhang, Wu, Norton, et al. 2018c). We note that in the current work, we are using subject data from the HCP, which are the same subjects from the same data source used in our previous work (Zhang, Wu, Norton, et al. 2018c). In this prior work, we performed parameter tuning for the HCP data for tractography of major parameters including fiber seeding fractional anisotropy and fiber stopping fractional anisotropy. We performed both quantitative analysis and quality control of the tractography streamline output and then selected the best-performing parameters, which we then used in our current work. Fibers that were longer than 40 mm were retained to avoid any bias toward implausible short fibers (Guevara et al. 2012; Jin et al. 2014; Lefranc et al. 2016). For each of the subjects under study, there were about 1 million fibers in the whole brain tractography. Visual and quantitative quality control of the tractography was performed using a quality control tool in the *whitematteranalysis* software http://github.com/SlicerDMRI/whitematteranalysis.

Fiber Clustering Methods

Cluster analysis. To enable the identification of fiber tract parcels (i.e., fiber clusters) from orbital, lateral, and medial prefrontal cortical regions projecting to the caudate, we used a data-driven fiber clustering atlas (Zhang, Wu, Norton, et al. 2018c). This atlas allows for a whole brain tractography parcellation into 2000 fiber clusters according to the white matter anatomy (i.e., fiber geometric trajectory).

To our knowledge, there is no agreed upon standard for parcellation scale in the literature and we believe that an absolute optimal scale is difficult to determine. We note, however, that we chose the 2000 fiber clusters because it provides a fine-scale parcellation of the whole brain tractography, which has been suggested by our prior work to be beneficial in modeling whole brain structural connectivity (Zhang, Savadjiev, et al. 2018a). Also, in our previous work (Zhang, Wu, Norton, et al. 2018c), we have shown this parcellation scale provided a good parcellation generation across different populations including groups of subjects across the lifespan from 1 day after birth up to 82 years old; that is, the corresponding white matter fiber clusters can be consistently identified across various subject groups. An additional area for future methodologic investigation would address whether changing cluster number would yield similar results. However, to test this would require regeneration of the fiber clustering atlas, itself, which would be outside the scope of the current work.

The clusters themselves were comprised of fibers, or streamlines, that reflect the principal direction of white matter axons

(see Fig. 1*a*,*b*). We have performed extensive data processing to remove potential false-positive fibers. We have included a data-driven outlier removal process to reject improbable fibers within a cluster. In this case, fibers that are not consistent across subjects are removed. We note that this is currently widely used in tractography analysis for false-positive fiber filtering and has been shown to be effective in multiple studies from our group (Zhang, Savadjiev, et al. 2018a; Zhang, Wu, Ning, et al. 2018b; Zhang et al. 2019; Zhang 2020).

In brief, the atlas was generated by creating dense tractography maps of 100 individual HCP subjects (an independent population from the HCP subjects used in the present study) and then applying a fiber clustering method to group the tracts across subjects according to their similarity in shape and location. For each cluster in the atlas, the tract anatomical profile (TAP) (Zhang, Wu, Norton, et al. 2018c), that is, the set of segmented brain FreeSurfer regions through which the cluster passed, is provided. The TAP was calculated based on the 100 HCP-atlas subjects, as described in Zhang, Wu, Norton, et al. (2018c). Briefly, for each cluster, the set of intersected FreeSurfer regions per subject was computed. Then, the set of regions (here, a given ROI in the PFC and the caudate) intersected by at least 40% of fiber streamlines of this cluster across all subjects was used to define the cluster's TAP. In this work, fiber clusters of interest from the cortex projecting to the caudate were identified according to their connected anatomical brain regions as defined in the TAP. In this way, we identified 17 white matter fiber clusters that connected the PFC and the caudate in both left and right hemispheres, which met the threshold of having at least 40% of its streamlines intersecting both the cortex and the caudate. The following FreeSurfer ROIs (Desikan et al. 2006) were used to identify the clusters of interest to generate the streamlines of interest: the caudalanteriorcingulate, caudalmiddlefrontal, lateralorbitofrontal, medialorbitofrontal, parsopercularis, parsorbitalis, parstriangularis, rostralanteriorcingulate, rostralmiddlefrontal, superiorfrontal, frontalpole cortical ROIs, and the caudate nucleus.

Intercluster streamline endpoint distance analysis. To quantify the topographical relationship of these fiber clusters, between each pair of fiber clusters, we measured the mean Euclidean distance between the endpoints of streamlines in the frontal cortex (i.e., the cortical intercluster, pairwise, endpoint distance) and the mean Euclidean distances between the endpoints of the streamlines in the corresponding fiber cluster pair in the caudate (i.e., the caudate intercluster, pairwise, endpoint distance). See Figs 1*a* and 2*a*,*b*. This, in turn, allowed us to quantify the degree of convergence or divergence, that is, deviation from a parallel, strictly topographic organization, among the 17 frontostriatal fiber cluster projections.

Statistical Analysis

To determine the overall pattern of frontostriatal connectivity, we generated scatter plots for each hemisphere (see Fig. S1) based on the 17 fiber clusters (with 136 pairs of fiber clusters, yielding 136 data points) that showed the relationship between the cortical distances and the corresponding striatal distances of the obtained fiber cluster pairs that connect the prefrontal cortex and the caudate. An exponential model was then fit to the data points that was compared with a linear model.

To determine the local variation of the pattern of frontostriatal connectivity in each hemisphere, we performed an additional analysis. First, we generated scatter plots (see Fig. S1) for each of the 17 clusters. For each cluster, we performed a paired *t*-test of the distance from that cluster to the other clusters in the hemisphere, comparing these mean intercluster streamline endpoint distances between the cortex and corresponding distances in the caudate. To determine significance, we then adjusted the *P* values for the 17 cortex to caudate comparisons within a hemisphere using a Bonferroni correction (*P* values were multiplied by 17).

We assessed the association between degree of convergence and streamline counts in fiber clusters using Spearman's rank correlation coefficients. For each cluster, we estimated the within hemisphere average over subjects of intercluster distances separately for the cortex and caudate. The difference of convergence is defined to be the difference in the values between the cortex and caudate. In order to obtain a standardized measure of convergence over subjects, we calculated a one sample t-statistic of the degree of convergence for each fiber cluster.

Results

Subject Demographics

Hundred young adult HSs were included in this study including forty-six males and fifty-four females. Subjects ranged in ages 22–35 years ($M = 29.00 \pm 3.51$), with an ethnic racial breakdown of 76% White, 19% Black or African American, 1% Asian, Native Hawaiian or Other Pacific Islander, 2% of more than one ethnicity reported, and 2% unreported. For completed years of education, 4% of the participants had 11 or fewer years of schooling, 19% 12 years, 7% 13 years, 9% 14 years, 4% 15 years, 41% had 16 years, and 16% had 17 or more years. Fluid intelligence fell in the average range $M = 102.34 \pm 17.29$.

The Overall Pattern of Frontostriatal Connectivity

To determine the overall pattern of frontostriatal connectivity in both hemispheres, we generated scatter plots in each hemisphere (see Fig. 4*a*,*b*) based on the 17 fiber clusters per hemisphere (with 136 pairs of fiber clusters, yielding 136 data points) that connect the prefrontal cortex and the caudate. These scatter plots showed the relationship between the cortical cluster endpoint distances and the corresponding caudate cluster endpoint distances of the obtained fiber cluster pairs. An exponential model was fit to the data points that was superior to a linear model in both hemispheres (see Fig. 4*a*,*b*). We showed that the PFC-caudate white matter streamline projection pattern was nonlinear, which was driven by the results from 10 cluster pairs (highlighted by the green circles located on the right lower portion of the scatter plot below and on the fitted curve in Fig. 4*a*,*b*). Of note, certain clusters, for example, cluster number 6 originating in inferior frontal gyrus (IFG), pars triangularis, were significantly overrepresented in these ten cluster pairs in both hemispheres. In fact, all these ten cluster pairs include cluster 6 as one of the pairs. We note that in Figure 4*a*,*b* the 16 green circles represent clusters that include cluster 6. Ten of these circles, all including cluster 6 as one of the pairs, drive the nonlinearity of our fitted curve.

Local Variation in the Pattern of Frontostriatal Connectivity

To determine the local variation of the pattern of frontostriatal connectivity in both left and right hemispheres, first, we

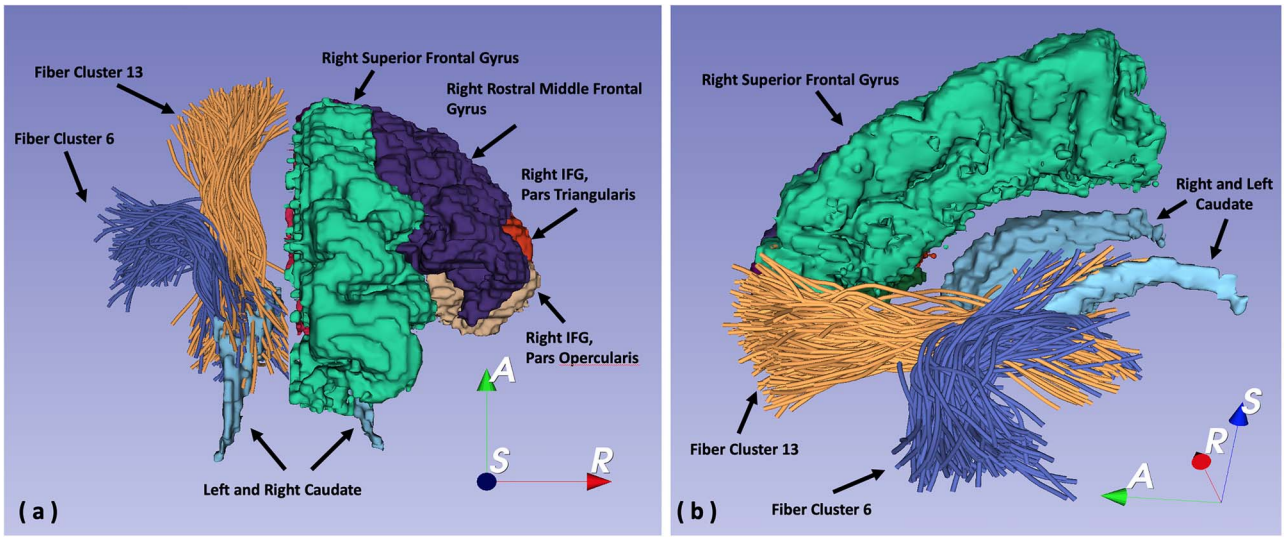

Figure 2. (*a*) 3D reconstruction of streamlines and regions of interest seen from a superior view of right hemisphere frontal cortex subregions and of fiber cluster 6, coming from IFG, pars triangularis, and of cluster 13, coming from rostral middle frontal gyrus. (*b*) 3D reconstruction of streamlines and regions of interest seen from a medial oblique view of right hemisphere superior frontal gyrus, left and right hemisphere caudate, and of the same fiber clusters, 6 and 13.

Table 1 Adjusted *t*-test *P* values for selective fiber clusters showing significant (and trend) patterns of frontostriatal convergence

Hemisphere	Fiber cluster number	FreeSurfer regions of interest	*t*-Test adjusted *P* values
Left	1	Rostralmiddlefrontal, superiorfrontal	0.10
Left	6	IFG, parstriangularis	0.0000012**
Left	8	IFG, parstriangularis	0.0043*
Left	9	Rostralmiddlefrontal	0.016*
Left	10	Medial and lateral orbitofrontal	0.061
Right	1	Rostralmiddlefrontal, superiorfrontal	0.067
Right	6	IFG, parstriangularis	0.0000011**
Right	8	IFG, parstriangularis	0.0051*
Right	9	Rostralmiddlefrontal	0.0080*
Right	10	Medial and lateral orbitofrontal	0.049*

Note: *$P < 0.05$
**$P < 0.001$

generated scatter plots for each of the 17 cluster pairs showing the relationship between cortical and striatal endpoint distances between that cluster and the other 16 (see Fig. S1). *t*-Tests comparing the mean intercluster endpoint distances in cortex and caudate between each cluster with the other 16 clusters revealed that fiber clusters coming from the ventrolateral (left and right hemisphere clusters 6 and 8), dorsolateral (left and right hemisphere cluster 9 with right hemisphere cluster 1 showing a trend), and orbitofrontal PFC (right hemisphere cluster 10 with left hemisphere cluster 10 showing a trend) showed significant convergence (i.e., caudate endpoint distance < cortex endpoint distance) after correcting for multiple tests (adjusted *P* value < 0.05). See Table 1 for the adjusted *t*-test *P* values for fiber clusters showing significant (and trend) patterns of frontostriatal convergence. See Figure 3 for 3D reconstructions of the fiber clusters showing significant convergence. See Figure 5 for the scatter plot of cluster 6 and see Figure S1 for the scatter plots of all fiber clusters. We also note that Figure 5*a*,*b* showing the scatter plot of clusters involving cluster 6 represent the same data points as the green circles in Figure 4*a*,*b*.

We also investigated the association between the degree of convergence and streamline counts in fiber clusters using Spearman's rank correlation coefficients. We calculated a one-sample *t*-statistic of the degree of convergence for each fiber cluster with the other clusters in each hemisphere and correlated this with the streamline counts in each cluster (see Methods section). We found the values for these correlations were nonsignificant in either the left hemisphere (rho = −.032; $P = 0.22$) or the right hemisphere (rho = −0.48; $P = 0.08$).

Discussion

We here present a study employing a novel use of diffusion imaging fiber cluster tractography to assess the organization of frontostriatal brain wiring in HSs. There are three principal findings in this study. First, we show that the overall PFC wiring connectivity pattern projecting from the PFC to the caudate deviates from a strictly topographic, parallel organization, due to a pattern of convergence in regionally specific anatomic fiber clusters connecting the PFC and striatum. Second, we identify

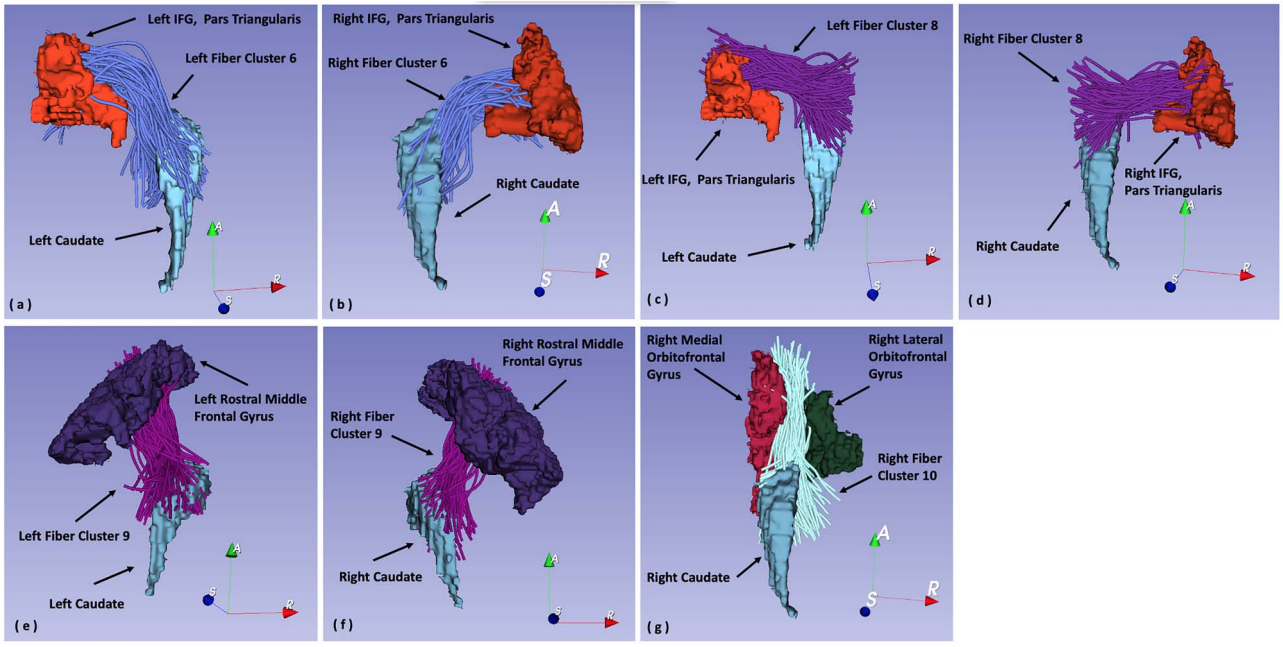

Figure 3. (*a*). 3D reconstruction of fiber cluster 6 projecting from left IFG, pars triangularis, to left caudate. (*b*) 3D reconstruction of fiber cluster 6 projecting from right IFG, pars triangularis, to right caudate. (*c*) 3D reconstruction of fiber cluster 8 projecting from left IFG, pars triangularis, to left caudate. (*d*) 3D reconstruction of fiber cluster 8 projecting from right IFG, pars triangularis, to right caudate. (*e*) 3D reconstruction of fiber cluster 9 projecting from left rostral middle frontal gyrus to left caudate. (*f*) 3D reconstruction of fiber cluster 9 projecting from right rostral middle frontal gyrus to right caudate. (*g*) 3D reconstruction of fiber cluster 10 projecting from right lateral and medial orbitofrontal cortex to the right caudate.

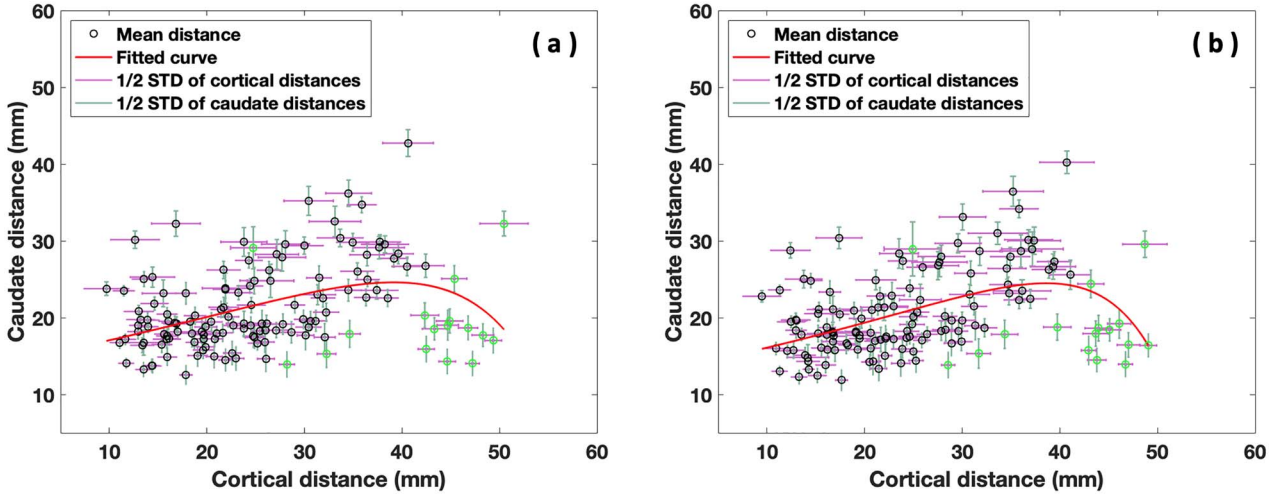

Figure 4. Scatter plots of the 17 fiber clusters per hemisphere (with 136 pairs of fiber clusters, yielding 136 data points) that connect the prefrontal cortex and the caudate, showing a nonlinear relationship between cortical and caudate intercluster streamline endpoint distances in the left, (*a*), and right, (*b*), hemispheres. The green circles represent all 16 cluster pairs with cluster 6 included as one of the cluster pair. Note, the 10 green circles located in the lower right portion of the scatter plot below and on the fitted curve drive the nonlinearity of the fitted curve.

the anatomic location in the PFC of these regionally specific fiber clusters with significant patterns of convergence. We found that these clusters originated in subregions in the ventrolateral, dorsolateral, and orbitofrontal PFC, that is, in the inferior frontal gyrus, pars triangularis, the rostral middle frontal gyrus, and the medial and lateral orbitofrontal gyri, respectively. Third, we show a similar bilateral organization of cortical projections to the caudate in both the left and right hemispheres including the specific clusters identified as convergent.

It is of value to understand the pattern of axonal outflow from the frontal cortex to the striatum, with the caudate representing a core part of the associative striatum, as it is an important component of the basal ganglia–cortical circuitry that permits the basal ganglia to modulate cortical function. The organization of corticostriatal anatomic connectivity has been thoroughly investigated through the use of animal tract tracing studies and more recently through the use of in vivo human brain imaging studies (Draganski et al. 2008; Haber 2011;

Levitt et al. 2020). For example, in an animal tract tracing study, Averbeck et al. (2014) found that the pattern of corticostriatal connectivity deviated from a strictly topographic one. They demonstrated this in monkeys by comparing the distance between pairs of injections in monkeys in the (prefrontal) cortex with the degree of overlap in the projection zones of these cortical injection sites. They found an exponential decrease in overlap in striatal projection zones as a function of greater distance between pairs of injection sites. They discussed that overlap in striatal projection zones was functionally important as this permitted the formation of hubs in target areas in the striatum that allow for the integration of information from input from functionally diverse cortical subregions. Although our data do not measure where fibers terminate inside the striatum, we interpret the comparison between the endpoint distances projecting to the surface of the striatum with the endpoint distances on the surface of the cortex to reflect a pattern of convergence of outflow from the prefrontal cortex which is similar to a pattern of projection zone overlap described by Averbeck et al. (2014). In healthy human subjects, Draganski et al. (2008), using probabilistic diffusion imaging, found convergent support for the presence of overlap in the projection zones in the striatum coming from prefrontal, premotor, and motor cortices.

There are additional monkey animal tract tracing studies that offer support in the literature for a nontopographic corticostriatal organization with corticostriatal projection zone overlap in the striatum. For example, Yeterian and Van Hoesen (1978) found that cortical regions that were reciprocally connected, including that between sensory and motor association cortex, partially projected to the same region of the caudate nucleus. In fact, they postulated this to be a general anatomic principle of cortical caudate connectivity. In a later study, Selemon and Goldman-Rakic (1985) also found evidence of overlap in the ventromedial striatum, which they described as mostly interdigitated. These authors noted, however, that they did not assess the dorsolateral striatum. More recently, Averbeck et al. (2014) studying monkeys reported that the medial rostral caudate nucleus was a subregion of the striatum that, in particular, received input from five separate prefrontal injection sites suggesting to these authors that it represented a hub-like subregion in the striatum. The above studies in nonhuman primates strongly support the idea that projection zone overlap is an anatomic feature that characterizes corticostriatal connectivity.

The corticobasal ganglia circuitry has been described to influence a number of important higher cognitive functions, in addition to its traditional role in influencing motor activity. Thus, characterizing its normal pattern of wiring may allow for a better understanding of the neural substrates for such functions. As our principal findings of convergence, which we surmise allows for greater circuit integration, are linked to fiber clusters coming from the lateral PFC (ventrolateral clusters 6 and 8 and dorsolateral cluster 9) and orbitofrontal PFC (cluster 10), we emphasize higher cognitive functions associated with these regions of the PFC. Such processes include goal-directed behavior, reward processing, and declarative and working memory (e.g., Redgrave et al. 2010; Borst and Anderson 2013; Haber and Behrens 2014), functions that can be influenced by activation or inhibition of the PFC or the caudate, part of the striatum, as this is an interconnected network.

The IFG, pars triangularis, in the ventrolateral PFC, which shows the strongest degree of convergence of our fiber clusters (see Figs 2*a*,*b* and 3*a*,*b*), is part of Broca's speech and language area (Dronkers et al. 2007; Skipper et al. 2007). The rostral middle frontal gyrus (rMFG), in the dorsolateral PFC, is a key node in executive function, which includes such functions as working memory and reward-based learning (Gold et al. 2008; Barch and Dowd 2010; Szczepanski and Knight 2014). Both the rMFG and the IFG have also been described as components in the executive control network that links dorsolateral frontal and parietal cortex (e.g., Seeley et al. 2007; Barch 2013). An alternative term for a network connecting frontal and parietal cortex is the frontoparietal network. In a meta-analysis of Borst and Anderson (2013) of the frontoparietal network, which they describe as including the dorsolateral prefrontal cortex, the anterior cingulate, and the intraparietal sulcus area, they showed that activity in the inferior frontal gyrus and the anterior cingulate was associated with declarative memory retrieval, while activity in the inferior parietal lobule, an area around the inferior frontal gyrus and in the anterior cingulate, was associated with updating of working memory. Of further interest, in a monkey study of Yeterian et al. (2012), they showed that the IFG, pars triangularis (area 45; ventrolateral PFC [VLPFC]), and rMFG (area 46/9; dorsolateral [DLPFC]) are highly anatomically interconnected. As noted above, Yeterian and Van Hoesen (1978) have suggested the anatomical principle that reciprocally connected cortical zones project in an overlapping manner onto the subcortical caudate. This is precisely what we demonstrated with PFC projections to the caudate where cluster 6, the IFG pars triangularis (VLPFC) cluster, is especially convergent with clusters coming from rMFG (DLPFC), for example, clusters 13 and 4 and 11 and 9. See Figure S1, the cluster 6 plots; and, also, see the cluster 6 plots as shown in Figure 5.

With regard to the orbitofrontal cortex (OFC), both human and animal studies provide evidence that the OFC helps to modulate goal-directed versus habitual behavior, behaviors that reflect both cognitive control and reward processing. For example, Yin et al. (2004, 2005) performed inactivation studies in rodents in which they showed that dorsolateral and dorsomedial striatum were associated with goal-directed versus habitual behavior, respectively. In a later study, Gremel and Costa (2013) showed that neuronal activity in the OFC and the dorsomedial striatum to which it projects were "more engaged" and the dorsolateral striatum "less engaged" during goal-directed actions. Also, when they chemogenetically inhibited the OFC in these mice, goal-directed action was decreased, whereas when they optogenetically activated the OFC, goal-directed action was increased (Gremel and Costa 2013). Furthermore, both human imaging and nonhuman primate studies reviewed by Redgrave et al. (2010) support that the OFC and its target in the striatum, for example, the dorsomedial striatum in humans and monkeys, are active during goal-directed behavior.

The above findings in animal and human studies highlight the importance of the IFG and OFC for memory, goal-directed behavior, and reward processing. This is of particular relevance for our results where we find in HSs that clusters coming from subregions in the ventrolateral (IFG, pars triangularis), dorsolateral (rostral middle frontal gyrus), and orbitofrontal (ventromedial and ventrolateral orbital gyri) PFC geometrically project to the caudate in a significantly convergent pattern (see Fig. S1). Furthermore, we find highly similar bilateral results for the overall geometric pattern of projections (see Fig. S1). As the hemispheric fiber cluster endpoint distance measures were independently derived, their validity is strengthened by the highly similar bilateral results. Our finding of a pattern of projection convergence, we believe, is consistent with a pattern of projection zone overlap at the level of the caudate. This, in

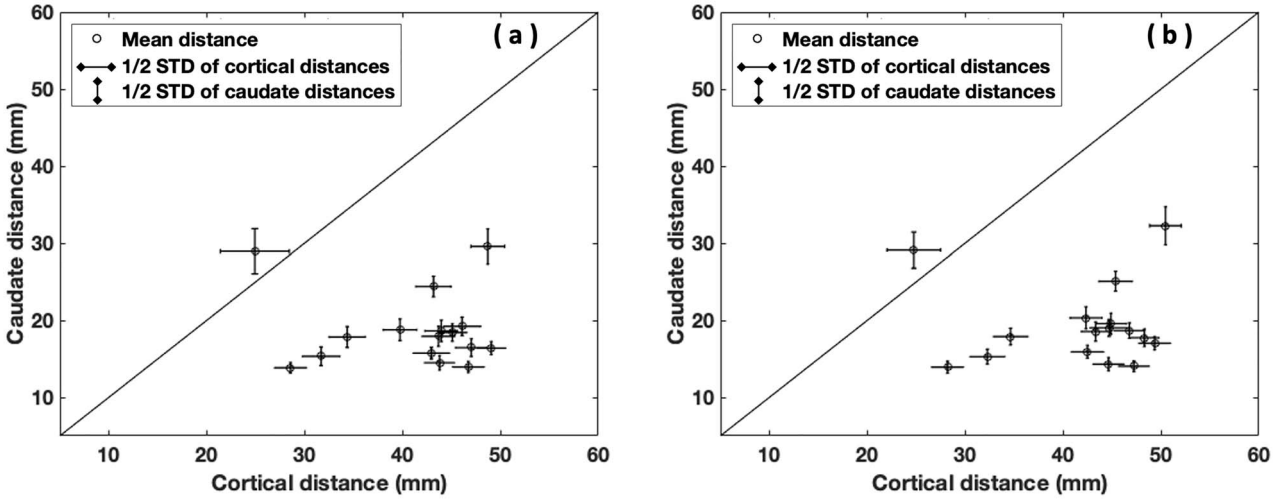

Figure 5. Scatter plot of cluster 6 originating in left and right hemisphere IFG, pars triangularis PFC, showing the relationship between cortical and caudate intercluster streamline endpoint distances between it and the other 16 clusters (left, (*a*), and right, (*b*), hemisphere *t*-test adjusted *P* values = 0.0000012; 0.0000011).

turn, would allow for the integration of information from cortical input at the level of the striatum, especially, as discussed above, in cortical regions that are interconnected.

In a prior study, using a different measure assessing the organization of frontostriatal connectivity, we showed an abnormal frontostriatal wiring pattern in chronic schizophrenia (Levitt et al. 2020). This study assessed the amount of striatal surface voxels receiving mixed cortical functional subregion input in chronic schizophrenia and in normal controls. We showed that chronic schizophrenia patients had fewer mixed voxels, that is, a less integrative pattern of connectivity, particularly in the left hemisphere associative striatum. As abnormal goal-directed behavior, reward processing, and memory may be important characteristics of schizophrenia (e.g., Gold et al. 2008; Barch and Dowd 2010), we surmise that abnormal wiring in frontostriatal circuitry, which may be a substrate for such functions, could contribute to such behavioral deficits.

Another important aspect of brain wiring is that as it occurs during development, measures of aberrant brain wiring using MRI tractography, thus, might serve as biological markers for normal as well as abnormal development. For example, such markers could be used to study developmental differences in the sexes that our group has begun to do in HSs. Also, for example, see Savadjiev et al. (2014) who examined white matter geometry using a measure of white matter dispersion and found abnormalities in a sexually dimorphic manner in adolescent onset schizophrenia. These authors suggested their white matter geometry measure potentially reflected neurodevelopmental differences between the sexes.

Limitations of the paper include that the design of the study is a cross-sectional one. Thus, the idea that the novel brain wiring measure we propose reflects neurodevelopment, ideally, should be confirmed in a longitudinal study assessing the trajectory of our findings starting in early childhood and extending into adulthood. An alternative strategy would be to test whether our measures remain stable over time. Also, the absence of clusters projecting to the caudate coming from rostral anterior cingulate gyrus is a limitation. Dorsal anterior cingulate fibers have been found in monkeys to project to the anterior caudate (e.g., Haber et al. 2006; Haber 2016). Our fiber clustering method, however, includes a requirement that only those streamlines that were longer than 40 mm were retained to eliminate implausibly short fiber tracts, but which may have led to the absence of such connections. Hence, this region may show convergent projections to the caudate, which our method would miss. However, if we do not eliminate the shorter fibers in our whole brain tractography, this will influence the clustering of the long-tract fibers, which we are most interested in for this study. An alternative strategy would be to eliminate longer-tract fibers and focus instead on shorter-tract fibers, but this raises the challenge of validating agreed upon shorter-tract fibers in the brain, which at this point is lacking in the literature.

An additional potential limitation is that individual streamlines within fiber clusters need not terminate directly onto the caudate in order to be counted in the endpoint calculations as described above in the Methods section. Lastly, we acknowledge the risk of false-negative and false-positive streamlines using dMRI tractography (e.g., Thomas et al. 2014; Maier-Hein et al. 2017).

In summary, employing a novel use of tractography, we show in HSs that the normal pattern of frontostriatal connectivity is characterized by regional nontopographic organization due to significantly increased convergence of fiber bundles emanating from selective PFC regions in the left and right hemispheres. Specifically, our main findings are that fiber clusters coming from subregions of limbic orbitofrontal PFC and associative ventrolateral and dorsolateral PFC, with a bilaterally similar pattern, project in a convergent manner onto the caudate. The consistency of our findings across both hemispheres is noteworthy. The finding raises the important issue of localization of hemispheric symmetry versus asymmetry and it should be explored in future studies in both sexes in healthy controls and in disease populations to test whether it will be replicated.

We believe the novelty of our approach lies in its use of diffusion imaging tractography to assess brain wiring rather than diffusivity. Hence, in our view, our measures could serve as biomarkers of early development both in healthy controls and in individuals with neuropsychiatric disorders. In addition, for future studies, it will also be important to apply these measures to subjects over the life span, from early childhood

to old age, to test their stability. Further, we plan to explore this circuitry in other neuropsychiatric disorders such as early psychosis to test support for our earlier finding of miswiring in chronic schizophrenia (Levitt et al. 2020). Once frontostriatal wiring patterns are established in healthy male and female subjects, such patterns can be examined in neurodevelopmental disorders in both males and females, particularly those affecting goal-directed behavior, reward processing, and memory such as schizophrenia. Further, given the importance of basal ganglia circuitry for higher cognitive functions, in particular with regard to memory, learning, and reward processing, possible brain wiring associations with tasks that assess such behavior also can be studied.

Supplementary Material

Supplementary material can be found at *Cerebral Cortex* online.

Funding

Grants from the National Institutes of Health (R21MH121704 (J.J.L.), R01MH119222 (PIs: Y.R., L.J.O.), P41EB015902 (PI: Kikinis, Westin), R01 MH074794 (Westin), R21MH116352 (Ning), K24MH110807, R01MH112748 (M.K.)); VA Merit Award (I01CX000176-06 to M.E.S.).

Notes

Conflict of Interest: None of the authors has conflicts of interest.

References

Alexander GE, Crutcher MD. 1990. Functional architecture of basal ganglia circuits: neural substrates of parallel processing. *Trends Neurosci*. 13(7):266–271.

Alexander GE, Crutcher MD, DeLong MR. 1990. Basal ganglia-thalamocortical circuits: parallel substrates for motor, oculomotor, "prefrontal" and "limbic" functions. *Prog Brain Res*. 85:119–146.

Alexander GE, DeLong MR, Strick PL. 1986. Parallel organization of functionally segregated circuits linking basal ganglia and cortex. *Annu Rev Neurosci*. 9:357–381.

Averbeck BB, Lehman J, Jacobson M, Haber SN. 2014. Estimates of projection overlap and zones of convergence within frontal-striatal circuits. *J Neurosci*. 34(29):9497–9505.

Barch DM. 2013. Brain network interactions in health and disease. *Trends Cogn Sci*. 17(12):603–605.

Barch DM, Dowd EC. 2010. Goal representations and motivational drive in schizophrenia: the role of prefrontal-striatal interactions. *Schizophr Bull*. 36(5):919–934.

Basser PJ, Pajevic S, Pierpaoli C, Duda J, Aldroubi A. 2000. In vivo fiber tractography using DT-MRI data. *Magn Reson Med*. 44(4):625–632.

Basser PJ, Pierpaoli C. 1996. Microstructural and physiological features of tissues elucidated by quantitative-diffusion-tensor MRI. *J Magn Reson B*. 111(3):209–219.

Bhatia KP, Marsden CD. 1994. The behavioural and motor consequences of focal lesions of the basal ganglia in man. *Brain*. 117(4):859–876.

Borst JP, Anderson JR. 2013. Using model-based functional MRI to locate working memory updates and declarative memory retrievals in the fronto-parietal network. *Proc Natl Acad Sci USA*. 110(5):1628–1633.

Calabresi P, De Murtas M, Bernardi G. 1997. The neostriatum beyond the motor function: experimental and clinical evidence. *Neuroscience*. 78(1):39–60.

Cummings JL. 1993. Frontal-subcortical circuits and human behavior. *Arch Neurol*. 50(8):873–880.

Descoteaux M, Angelino E, Fitzgibbons S, Deriche R. 2007. Regularized, fast, and robust analytical Q-ball imaging. *Magn Reson Med*. 58(3):497–510.

Desikan RS, Segonne F, Fischl B, Quinn BT, Dickerson BC, Blacker D, Buckner RL, Dale AM, Maguire RP, Hyman BT, et al. 2006. An automated labeling system for subdividing the human cerebral cortex on MRI scans into gyral based regions of interest. *Neuroimage*. 31(3):968–980.

Draganski B, Kherif F, Kloppel S, Cook PA, Alexander DC, Parker GJ, Deichmann R, Ashburner J, Frackowiak RS. 2008. Evidence for segregated and integrative connectivity patterns in the human basal ganglia. *J Neurosci*. 28(28):7143–7152.

Dronkers NF, Plaisant O, Iba-Zizen MT, Cabanis EA. 2007. Paul Broca's historic cases: high resolution MR imaging of the brains of Leborgne and Lelong. *Brain*. 130(5):1432–1441.

Fillard P, Descoteaux M, Goh A, Gouttard S, Jeurissen B, Malcolm J, Ramirez-Manzanares A, Reisert M, Sakaie K, Tensaouti F, et al. 2011. Quantitative evaluation of 10 tractography algorithms on a realistic diffusion MR phantom. *Neuroimage*. 56(1):220–234.

Fischl B. 2012. FreeSurfer. *Neuroimage*. 62(2):774–781.

Glasser MF, Sotiropoulos SN, Wilson JA, Coalson TS, Fischl B, Andersson JL, Xu J, Jbabdi S, Webster M, Polimeni JR, et al. 2013. The minimal preprocessing pipelines for the human connectome project. *Neuroimage*. 80:105–124.

Gold JM, Waltz JA, Prentice KJ, Morris SE, Heerey EA. 2008. Reward processing in schizophrenia: a deficit in the representation of value. *Schizophr Bull*. 34(5):835–847.

Gremel CM, Costa RM. 2013. Orbitofrontal and striatal circuits dynamically encode the shift between goal-directed and habitual actions. *Nat Commun*. 4(1):2264.

Guevara P, Duclap D, Poupon C, Marrakchi-Kacem L, Fillard P, Le Bihan D, Leboyer M, Houenou J, Mangin JF. 2012. Automatic fiber bundle segmentation in massive tractography datasets using a multi-subject bundle atlas. *Neuroimage*. 61(4):1083–1099.

Haber SN. 2003. The primate basal ganglia: parallel and integrative networks. *J Chem Neuroanat*. 26(4):317–330.

Haber SN. 2010. Convergence of limbic, cognitive, and motor cortico-striatal circuits with dopamine pathways in primate brain. In: Iversen LL, Iversen SD, Dunnett SB, Bjorklund A, editors. *Dopamine handbook*. Oxford: Oxford University Press, Inc., pp. 38–48.

Haber SN. 2011. Neuroanatomy of reward: a view from the ventral striatum. In: Gottfried JA, editor. *Neurobiology of sensation and reward*. Boca Raton (FL): CRC Press.

Haber SN. 2016. Corticostriatal circuitry. *Dialogues Clin Neurosci*. 18(1):7–21.

Haber SN, Behrens TE. 2014. The neural network underlying incentive-based learning: implications for interpreting circuit disruptions in psychiatric disorders. *Neuron*. 83(5):1019–1039.

Haber SN, Kim KS, Mailly P, Calzavara R. 2006. Reward-related cortical inputs define a large striatal region in primates

that interface with associative cortical connections, providing a substrate for incentive-based learning. *J Neurosci*. 26(32):8368–8376.

Jin Y, Shi Y, Zhan L, Gutman BA, de Zubicaray GI, McMahon KL, Wright MJ, Toga AW, Thompson PM. 2014. Automatic clustering of white matter fibers in brain diffusion MRI with an application to genetics. *Neuroimage*. 100:75–90.

Lefranc S, Roca P, Perrot M, Poupon C, Le Bihan D, Mangin JF, Riviere D. 2016. Groupwise connectivity-based parcellation of the whole human cortical surface using watershed-driven dimension reduction. *Med Image Anal*. 30:11–29.

Lehericy S, Ducros M, Van de Moortele PF, Francois C, Thivard L, Poupon C, Swindale N, Ugurbil K, Kim DS. 2004. Diffusion tensor fiber tracking shows distinct corticostriatal circuits in humans. *Ann Neurol*. 55(4):522–529.

Levitt JJ, Kubicki M, Nestor PG, Ersner-Hershfield H, Westin CF, Alvarado JL, Kikinis R, Jolesz FA, McCarley RW, Shenton ME. 2010. A diffusion tensor imaging study of the anterior limb of the internal capsule in schizophrenia. *Psychiatry Res*. 184(3):143–150.

Levitt JJ, McCarley RW, Dickey CC, Voglmaier MM, Niznikiewicz MA, Seidman LJ, Hirayasu Y, Ciszewski AA, Kikinis R, Jolesz FA, et al. 2002. MRI study of caudate nucleus volume and its cognitive correlates in neuroleptic-naive patients with schizotypal personality disorder. *Am J Psychiatry*. 159(7): 1190–1197.

Levitt JJ, Nestor PG, Kubicki M, Lyall AE, Zhang F, Riklin-Raviv T, LJ OD, McCarley RW, Shenton ME, Rathi Y. 2020. Miswiring of frontostriatal projections in schizophrenia. *Schizophr Bull*. 46(4):990–998.

Levitt JJ, Nestor PG, Levin L, Pelavin P, Lin P, Kubicki M, McCarley RW, Shenton ME, Rathi Y. 2017. Reduced structural connectivity in frontostriatal white matter tracts in the associative loop in schizophrenia. *Am J Psychiatry*. 174(11): 1102–1111.

Maier-Hein KH, Neher PF, Houde JC, Cote MA, Garyfallidis E, Zhong J, Chamberland M, Yeh FC, Lin YC, Ji Q, et al. 2017. The challenge of mapping the human connectome based on diffusion tractography. *Nat Commun*. 8(1):1349.

Malcolm JG, Shenton ME, Rathi Y. 2010. Filtered multitensor tractography. *IEEE Trans Med Imaging*. 29(9): 1664–1675.

Manoach DS, Gollub RL, Benson ES, Searl MM, Goff DC, Halpern E, Saper CB, Rauch SL. 2000. Schizophrenic subjects show aberrant fMRI activation of dorsolateral prefrontal cortex and basal ganglia during working memory performance. *Biol Psychiatry*. 48(2):99–109.

Mori S, Crain BJ, Chacko VP, van Zijl PC. 1999. Three-dimensional tracking of axonal projections in the brain by magnetic resonance imaging. *Ann Neurol*. 45(2):265–269.

Ning L, Laun F, Gur Y, DiBella EV, Deslauriers-Gauthier S, Megherbi T, Ghosh A, Zucchelli M, Menegaz G, Fick R, et al. 2015. Sparse reconstruction challenge for diffusion MRI: validation on a physical phantom to determine which acquisition scheme and analysis method to use? *Med Image Anal*. 26(1):316–331.

O'Donnell LJ, Suter Y, Rigolo L, Kahali P, Zhang F, Norton I, Albi A, Olubiyi O, Meola A, Essayed WI, et al. 2017. Automated white matter fiber tract identification in patients with brain tumors. *Neuroimage Clin*. 13:138–153.

Rathi Y, Malcolm JG, Michailovich O, Westin CF, Shenton ME, Bouix S. 2010. Tensor kernels for simultaneous fiber model estimation and tractography. *Magn Reson Med*. 64(1): 138–148.

Redgrave P, Rodriguez M, Smith Y, Rodriguez-Oroz MC, Lehericy S, Bergman H, Agid Y, DeLong MR, Obeso JA. 2010. Goal-directed and habitual control in the basal ganglia: implications for Parkinson's disease. *Nat Rev*. 11(11): 760–772.

Rushworth MF, Noonan MP, Boorman ED, Walton ME, Behrens TE. 2011. Frontal cortex and reward-guided learning and decision-making. *Neuron*. 70(6):1054–1069.

Savadjiev P, Whitford TJ, Hough ME, Clemm von Hohenberg C, Bouix S, Westin CF, Shenton ME, Crow TJ, James AC, Kubicki M. 2014. Sexually dimorphic white matter geometry abnormalities in adolescent onset schizophrenia. *Cereb Cortex*. 24:1389–1396.

Seeley WW, Menon V, Schatzberg AF, Keller J, Glover GH, Kenna H, Reiss AL, Greicius MD. 2007. Dissociable intrinsic connectivity networks for salience processing and executive control. *J Neurosci*. 27(9):2349–2356.

Selemon LD, Goldman-Rakic PS. 1985. Longitudinal topography and interdigitation of corticostriatal projections in the rhesus monkey. *J Neurosci*. 5(3):776–794.

Skipper JI, Goldin-Meadow S, Nusbaum HC, Small SL. 2007. Speech-associated gestures, Broca's area, and the human mirror system. *Brain Lang*. 101(3):260–277.

Szczepanski SM, Knight RT. 2014. Insights into human behavior from lesions to the prefrontal cortex. *Neuron*. 83(5): 1002–1018.

Thomas C, Ye FQ, Irfanoglu MO, Modi P, Saleem KS, Leopold DA, Pierpaoli C. 2014. Anatomical accuracy of brain connections derived from diffusion MRI tractography is inherently limited. *Proc Natl Acad Sci USA*. 111(46): 16574–16579.

Voorn P, Vanderschuren LJ, Groenewegen HJ, Robbins TW, Pennartz CM. 2004. Putting a spin on the dorsal-ventral divide of the striatum. *Trends Neurosci*. 27(8):468–474.

Westin CF, Maier SE, Khidhir B, Everett P, Jolesz FA, Kikinis R. 1999. Image processing for diffusion tensor magnetic resonance imaging. In: *International Conference on Medical Image Computing and Computer-Assisted Intervention*. Springer, Berlin, Heidelberg: Springer, pp. 441–452.

Yeterian EH, Pandya DN, Tomaiuolo F, Petrides M. 2012. The cortical connectivity of the prefrontal cortex in the monkey brain. *Cortex*. 48(1):58–81.

Yeterian EH, Van Hoesen GW. 1978. Cortico-striate projections in the rhesus monkey: the organization of certain cortico-caudate connections. *Brain Res*. 139(1):43–63.

Yin HH, Knowlton BJ, Balleine BW. 2004. Lesions of dorsolateral striatum preserve outcome expectancy but disrupt habit formation in instrumental learning. *Eur J Neurosci*. 19(1): 181–189.

Yin HH, Knowlton BJ, Balleine BW. 2005. Blockade of NMDA receptors in the dorsomedial striatum prevents action-outcome learning in instrumental conditioning. *Eur J Neurosci*. 22(2):505–512.

Zhang F, Hoffmann N, Karayumak SC, Rathi Y, Golby AJ, O'Donnell LJ. 2020. Deep white matter analysis (DeepWMA): Fast and consistent tractography segmentation. *Med Image Anal*. 65:101761.

Zhang F, Norton I, Cai W, Song Y, Wells WM, O'Donnell LJ. 2017. Comparison between two white matter segmentation strategies: an investigation into white matter segmentation

consistency. In: *IEEE 14th International Symposium on Biomedical Imaging (ISBI 2017)*. p 796–799. IEEE.

Zhang F, Savadjiev P, Cai W, Song Y, Rathi Y, Tunc B, Parker D, Kapur T, Schultz RT, Makris N, et al. 2018a. Whole brain white matter connectivity analysis using machine learning: an application to autism. *Neuroimage*. 172: 826–837.

Zhang F, Wu W, Ning L, McAnulty G, Waber D, Gagoski B, Sarill K, Hamoda HM, Song Y, Cai W, et al. 2018b. Suprathreshold fiber cluster statistics: leveraging white matter geometry to enhance tractography statistical analysis. *Neuroimage*. 171:341–354.

Zhang F, Wu Y, Norton I, Rathi Y, Golby AJ, O'Donnell LJ. 2019. Test-retest reproducibility of white matter parcellation using diffusion MRI tractography fiber clustering. *Hum Brain Mapp*. 40(10):3041–3057.

Zhang F, Wu Y, Norton I, Rigolo L, Rathi Y, Makris N, O'Donnell LJ. 2018c. An anatomically curated fiber clustering white matter atlas for consistent white matter tract parcellation across the lifespan. *Neuroimage*. 179:429–447.